On the generation of preferential Λdoublet populations in the collisional relaxation of highly rotationally excited CH(X 2Π)

Millard H. Alexander and Paul J. Dagdigian

Citation: The Journal of Chemical Physics **101**, 7468 (1994); doi: 10.1063/1.468269
View online: http://dx.doi.org/10.1063/1.468269
View Table of Contents: http://scitation.aip.org/content/aip/journal/jcp/101/9?ver=pdfcov
Published by the AIP Publishing

On the generation of preferential Λ-doublet populations in the collisional relaxation of highly rotationally excited CH($X\ ^2\Pi$)

Millard H. Alexander
Department of Chemistry and Biochemistry, University of Maryland, College Park, Maryland 20742-2021

Paul J. Dagdigian
Department of Chemistry, The Johns Hopkins University, Baltimore, Maryland 21218-2685

(Received 24 June 1994; accepted 15 July 1994)

By means of full quantum close-coupling and coupled states calculations based on an *ab initio* potential energy surface for the Ar–CH system, we confirm a propensity seen experimentally by Hancock, Stuhl, and their co-workers. During the rotational relaxation of high rotational levels of the CH($X\ ^2\Pi$) radical, produced by photolysis of a suitable precursor, there appears a clear population imbalance in favor of the Λ-doublet levels of $\Pi(A'')$ symmetry. A full kinetic simulation, based on the calculated cross sections, reproduces nearly quantitatively the experimental observations of both the temporal evolution and the pressure dependence of this Λ-doublet asymmetry. This asymmetry is a consequence of both an enhanced depletion of high N $\Pi(A')$ levels and the enhanced formation of $\Pi(A'')$ levels in the next lower $(N-1)$ manifolds. The physical origin of this propensity involves a crossing between two adiabatic bender potentials which follow, respectively, the A' and A'' potential energy surface (PES). This crossing occurs only for the "helicopter-like" approach of the CH molecule, in which its rotational angular momentum is aligned along the initial relative velocity vector. Thus, a strong v, N correlation in the reactant channel results in a strong Λ, N correlation in the product channel.

I. INTRODUCTION

There is now a considerable body of experimental information available on state-to-state rotationally inelastic collisions of diatomic molecules in open-shell electronic states.[1] The most intensively studied are molecules in $^2\Pi$ electronic states. There have been similar advances in our theoretical understanding of inelastic collisions of molecules in $^2\Pi$ states. The general quantum formalism for such collisions has been worked out[2,3] and applied to the computation of cross sections involving a number of $^2\Pi$ molecules, including OH($X\ ^2\Pi$),[4–7] NO($X\ ^2\Pi$),[8–11] CH($X\ ^2\Pi$),[12] CaF($A\ ^2\Pi$),[13] CN($X\ ^2\Sigma^+$,$A\ ^2\Pi$),[14,15] and N_2^+($X\ ^2\Sigma_g^+$,$A\ ^2\Pi_u$).[16]

Because of the orbital degeneracy of $\Lambda \geqslant 1$ electronic states, the rotational/fine-structure levels appear as closely spaced *e*- and *f*-labeled[17] Λ doublets. With the approach of a structureless atomic collision partner, this orbital degeneracy is lifted, so that a correct description of the atom–molecule interaction requires *two* potential energy surfaces (PESs), of A' and A'' symmetry, which are degenerate only in linear geometry. In the Hund's case (a) coupling limit, which applies when the spin–orbit splitting is much larger than the rotational spacings, a formal quantum analysis[2] predicts that the inelastic cross sections should be unchanged upon reversal of the *e/f* labeling of the initial and final states. Thus, in the case (a) limit, if a pair of Λ-doublet levels is initially populated equally, then collisions cannot lead to an asymmetry in the final Λ-doublet populations.

By contrast, as the molecular coupling scheme approaches the Hund's case (b) limit, this symmetry no longer holds. Dagdigian *et al.*[18] have examined the general formalism for inelastic scattering of $^2\Pi$[case (b)] molecules in some detail. They have shown that Λ-doublet asymmetries in cross sections for transitions out of low-J levels can be a manifestation of quantum interference between the A' and A'' PESs. As a specific example, Alexander *et al.*[12] used *ab initio* PESs[19] to calculate CH($X\ ^2\Pi$)–He inelastic cross sections for comparison with experimental measurements by Macdonald and Liu.[20] If the initial state consisted of equal Λ-doublet populations in the lowest rotational level ($J=1/2$ F_2), as was approximately the case in the experiments of Macdonald and Liu,[20] the $\Pi(A'')$[21] Λ-doublet levels were predicted to be preferentially populated in *upward* transitions. By contrast, for the *downward* $J=3/2$ $F_1 \rightarrow J=1/2$ F_2 transition, the $\Pi(A')$ levels are preferred. In both cases the favored final Λ-doublet level could be predicted by assuming that the strength of a transition into a particular final state was governed by the magnitude of the matrix element of the interaction potential which couples the particular pair of initial and final states. Such an assumption is, of course, justified in the weak coupling limit, for which a first Born approximation would be expected to be applicable.

The above analysis was carried out for low rotational levels of CH($X\ ^2\Pi$), for which the energy gaps are generally much smaller than the translational energy, so that energy sudden conditions[22] apply. Hancock and co-workers[23,24] are currently investigating the relaxation of CH($X\ ^2\Pi$) radicals formed in the two-photon UV photolysis of ketene. At a photolysis wavelength of 279.3 nm, the nascent radicals are produced with considerable rotational excitation (most probable $N \approx 12$), but with equal populations in each pair of Λ-doublet populations.[23] However, subsequent relaxation of the nascent distribution by collisions with argon leads to preferential Λ-doublet populations in $\Pi(A'')$ levels.[24] Similar results have been found by Heinrich and Stuhl[25] for the collisional relaxation of CH($X\ ^2\Pi$) fragments produced in the 193 nm photolysis of CH_2Br_2. Relaxation studies, as a

 0021-9606/94/101(9)/7468/12/$6.00

function of both time and buffer gas (Ar) pressure, showed preferential population of the $\Pi(A'')$ levels. In unpublished experiments, Winterbottom and Reisler[26] have also made similar observations.

In the present paper we use quantum scattering calculations, based on our new Ar–CH(X) PESs,[27] to calculate cross sections for the rotational relaxation of CH(X) in high rotational states. These cross sections, as well as a subsequent full kinetic analysis, confirm the propensity observed by Hancock, Stuhl, and their co-workers. Specifically, for high-N levels of CH(X) in collisions with Ar, where the energy gaps are larger than thermal energy, the largest relaxation cross sections correspond to $\Delta N=-1$ transitions out of levels which have A' reflection symmetry (F_1e or F_2f) into levels which have A'' reflection symmetry (F_1f or F_2e). Thus, in the relaxation process $\Pi(A')$ levels are preferentially depleted, and $\Pi(A'')$ levels are preferentially populated. Further analysis shows that this relaxation specificity is a manifestation of avoided crossings between the sets of adiabatic bender curves[28] which correlate asymptotically with the successive $(N,N-1)$ rotational levels of the isolated CH(X) molecule. In a mechanism similar to what was proposed many years ago by Nikitin and co-workers,[29] in the presence of two PESs of different topology,[27] attractive adiabatic bender curves emanating from a higher rotational level can cross repulsive curves emanating from a lower rotational level, hence facilitating the relaxation process.

This paper is organized as follows: Section II presents a brief review of the quantum theory for rotationally inelastic collisions of a diatomic molecule in a $^2\Pi$ electronic state. In Sec. III state-to-state cross sections for collisions of CH($X\ ^2\Pi$) with Ar, which have been calculated using our recently obtained Ar–CH(X) PESs, are presented. Section IV presents a physical model which rationalizes the Λ-doublet propensities manifest in the calculated inelastic cross sections involving high-N rotational levels. These cross sections are used in Sec. V for a kinetic simulation of the collisional relaxation of rotationally excited CH($X\ ^2\Pi$) radicals studied experimentally by Hancock, Stuhl, and their coworkers. Section VI concludes with some general observations about the dynamics of inelastic collisions of open-shell diatomics.

II. THEORY OF ROTATIONALLY INELASTIC COLLISIONS OF $^2\Pi$ ELECTRONIC STATES

The quantum theory of rotationally inelastic collisions of a diatomic molecule in a $^2\Pi$ molecule has been presented previously.[2,3,10,18] We repeat here only those details which will be directly relevant in the ensuing discussion.

We express the diatomic wave functions in a symmetrized case (a) basis[30–32]:

$$|JM\Omega\epsilon\rangle=2^{-1/2}[|JM\Omega\rangle|\Lambda S\Sigma\rangle + \epsilon|JM-\Omega\rangle|-\Lambda S-\Sigma\rangle]. \quad (1)$$

Here J represents the total angular momentum with projections M and Ω along the space- and molecule-fixed z axes, respectively, and Σ and Λ denote the projections of the electronic spin and orbital angular momenta along the molecule-fixed z axis ($S=1/2$ and $\Lambda=1$). The symmetry index can take values $\epsilon=\pm1$. For a state of doublet spin multiplicity, we have $\epsilon=+1$ for e levels and $\epsilon=-1$ for f levels.[17]

The correct molecular wave functions are expressed as linear combinations of the symmetrized case (a) basis functions given in Eq. (1). We write

$$|JMF_i\epsilon\rangle=\sum_{\Omega} C^{\Omega}_{JF_i\epsilon}|JM\Omega\epsilon\rangle. \quad (2)$$

The expansion coefficients $C^{\Omega}_{JF_i\epsilon}$ are obtained by diagonalization of the Hamiltonian of the isolated CH molecule.[30–32] Eigenfunctions of a given J and parity are conventionally labeled F_1 and F_2 in order of increasing energy.[33] Since the spin–orbit constant A is comparable to the rotational constant B for CH($X\ ^2\Pi$),[34] the coupling scheme for this state is close to case (b) for all values of J. In the case (b) limit, we designate the total angular momentum exclusive of spin by N, and we have $J=N+1/2$ for F_1 levels and $J=N-1/2$ for F_2 levels. In the high-J limit, the magnitude of the coefficients $C^{\Omega}_{JF_i\epsilon}$ approaches $2^{-1/2}$, and the wave functions are equal admixtures of the case (a) $\Omega=1/2$ and 3/2 basis functions.

The interaction of CH in its $X\ ^2\Pi$ electronic state with Ar gives rise to two PESs, of A' and A'' reflection symmetry.[3] These PESs are functions of the Jacobi coordinates: r, the diatom internuclear separation; R, the separation of the centers of mass of the collision partners; and θ, the angle between $\hat{R}$ and $\hat{r}$. In what follows, we shall assume that r is fixed at the diatom equilibrium separation. We note, further, that $\hat{R}$ defines the body-frame z axis.

The inelastic collision dynamics are treated by expanding the ArCH wave function in the standard close-coupled (CC) expansion[2,35] in a basis $|JF_i\epsilon L\mathcal{J}\mathcal{M}\rangle$ of eigenfunctions of the total angular momentum $\mathcal{J}$, and $\mathcal{M}$, its projection on the space-fixed z axis. We write

$$\Psi^{\mathcal{J}\mathcal{M}}=(1/R)\sum_{JF_iL\epsilon} C^{\mathcal{J}}_{JF_i\epsilon L}(R)|JF_i\epsilon L\mathcal{J}\mathcal{M}\rangle, \quad (3)$$

where L is the orbital angular momentum. The expansion coefficients, which we designate as $C^{\mathcal{J}}_{JF_i\epsilon L}$, satisfy the standard close-coupled (CC) equations.[2,35] In matrix notation these are

$$\left[\frac{d^2}{dR^2}-W(R)\right]C^{\mathcal{J}}(R)=0, \quad (4)$$

where

$$W(R)\equiv\frac{L(L+1)}{2\mu R^2}+k^2-\frac{2\mu}{\hbar^2}V(R). \quad (5)$$

Here $L(L+1)$ and k^2 designate the diagonal matrices of the centrifugal potential and wave vectors of the individual coupled channels, respectively, and $V(R)$ is the full matrix of the interaction potential(s). The explicit form of the $V(R)$ in the space-fixed (SF) $|JF_i\epsilon L\mathcal{J}\mathcal{M}\rangle$ basis is given in the Appendix, where we correct some typographical errors in a previous paper.[18]

From the asymptotic form of the expansion coefficients, one obtains the S matrix, and subsequently the inelastic cross sections, as follows:

$$\sigma(JF_i\epsilon\rightarrow J'F_i'\epsilon')$$

$$=\frac{\pi}{(2J+1)k_J^2}\sum_{L,L',\mathscr{J}}(2\mathscr{J}+1)|S^{\mathscr{J}}(JF_i\epsilon L\mathscr{J},$$

$$J'F_i'\epsilon'L'\mathscr{J})|^2. \tag{6}$$

The expansion typically used in the CC treatment involves space-fixed (SF) orbital and molecular angular momentum states. Equivalently, one can use states in which the angular momentum refers to the body-fixed (BF) frame, an approach advocated years ago in the quantum treatment of molecular collisions[36–38] and, more recently, in the study of atom–diatom van der Waals molecules.[39,40] We define the BF frame by the orientation of **R**. In this case the expansion in Eq. (3) becomes

$$\Psi^{\mathscr{J}\mathscr{M}}=(1/R)\sum_{JF_i\epsilon P}C^{\mathscr{J}}_{JF_i\epsilon P}(R)|JF_i\varepsilon P\mathscr{J}\mathscr{M}\rangle, \tag{7}$$

where, consistent with the notation of Dubernet *et al.*,[41] we use P to denote the body frame projection of **J**. Since the orbital angular momentum vector **L** must be perpendicular to the triatomic plane, it follows that P is also the body frame projection of the *total* angular momentum $\mathscr{J}$.

The transformation between the body and space frame basis is diagonal in J and ϵ and given by[28,42]

$$|JF_i\epsilon P\mathscr{J}\mathscr{M}\rangle=\sum_L(-1)^{J-L+P}[2L+1]^{1/2}$$

$$\times\begin{pmatrix}J & L & \mathscr{J}\\ P & 0 & -P\end{pmatrix}|JF_i\epsilon L\mathscr{J}\mathscr{M}\rangle, \tag{8}$$

where (:::) is a $3j$ symbol.[43] The matrix of the interaction potential in the BF basis, also given in the Appendix, is block diagonal in the projection quantum number P. For future reference we shall denote each block of this matrix as W_P. In the centrifugal-decoupling (CD, also called "coupled states") approximation,[37,44] the BF equations, after Coriolis coupling is neglected, are additionally modified by replacement of the true diagonal centrifugal barrier[38,45]

$$\hbar^2[\mathscr{J}(\mathscr{J}+1)+J(J+1)-2P^2]/2\mu R^2, \tag{9}$$

by the diagonal matrix

$$\hbar^2\bar{L}(\bar{L}+1)/2\mu R^2, \tag{10}$$

where $\bar{L}$ is an effective angular momentum, taken to be the same for all channels. In terms of the CD S-matrix elements, the inelastic integral cross section is given by

$$\sigma(JF_i\epsilon\rightarrow J'F_i'\epsilon')=\sum_{P,\bar{L}}\sigma^{\bar{L},P}(JF_i\epsilon\rightarrow J'F_i'\epsilon'), \tag{11}$$

where the partial cross section is defined by

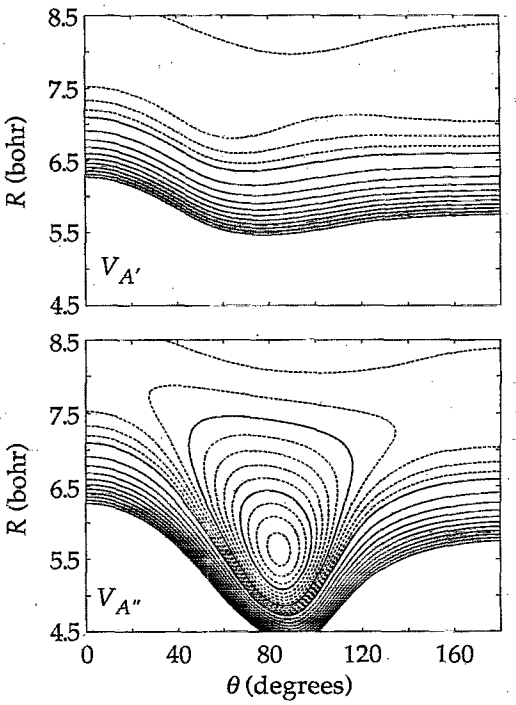

FIG. 1. Contour plots of the ArCH(X) PESs for the states of A' (upper panel) and A'' (lower panel) reflection symmetry, taken from Fig. 4 of Ref. 27. The linear CHAr geometry corresponds to θ=0°. The dashed contours indicate negative energies with the first contour at -10 cm^{-1} and a spacing of 10 cm^{-1}. The solid contours designate positive energy; the contours are equally spaced with the first contour at 50 cm^{-1}, a spacing of 50 cm^{-1}, and the last (innermost) contour at 500 cm^{-1}. For clarity, the contours at 0, -100, and -200 cm^{-1} are drawn with heavy solid curves.

$$\sigma^{\bar{L},P}(JF_i\epsilon\rightarrow J'F_i'\epsilon')$$

$$=\frac{\pi}{(2J+1)k_J^2}(2\bar{L}+1)|S^{\bar{L}}(JF_i\epsilon P,J'F_i'\epsilon'P)|^2. \tag{12}$$

III. COMPUTED CH($X\,^2\Pi$)–Ar CROSS SECTIONS

Recently, we determined[27] *ab initio* PESs for the interaction of CH($X\,^2\Pi$) with argon in order to assign the observed[46] electronic spectrum of the ArCH($X\,^2\Pi$) van der Waals complex. In the present treatment we use the PESs from Ref. 27, which were modified to compensate for the slight underestimate of the well depth in the raw *ab initio* data. With these modified PESs,[28] good agreement was found with experimental values[46] of both the dissociation energy and rotational constant in the lowest vibrational level of the ArCH(X) complex.

Figure 1 displays a contour plot of the ArCH(X) PESs used here. Qualitatively, the A'' PES has a relatively deep minimum at near perpendicular geometry (D_e=268 cm^{-1}, R_e=5.64 bohr). The A' PES has two much shallower minima at ArCH angles of 53° and 180°. The minima are located at larger Ar–CH distances (7.41 and 7.56 bohr, respectively) and the dissociation energies are smaller (D_e=78 and 76 cm^{-1}, respectively). The matrix elements of the interaction potential in Eq. (5), which are given explicitly

TABLE I. Comparison of coupled-states (upper entries) with close-coupled (lower entries) CH($X\ ^2\Pi$)–Ar cross sections (in Å^2) for $\Delta N=-1$ fine-structure conserving transitions at an incident translational energy of 300 cm^{-1}.

Initial N	$e\rightarrow e$	$f\rightarrow f$	$e\rightarrow f$	$f\rightarrow e$	$e\rightarrow e$	$f\rightarrow f$	$e\rightarrow f$	$f\rightarrow e$
	$F_1\rightarrow F_1$				$F_2\rightarrow F_2$			
	$\Pi(A')$[a]	$\Pi(A'')$	$\Pi(A'')$	$\Pi(A')$	$\Pi(A'')$	$\Pi(A')$	$\Pi(A')$	$\Pi(A'')$
8	0.57	1.82	5.08	1.28	1.66	0.53	1.40	4.75
	0.69	1.92	5.65	1.48	1.77	0.66	1.64	5.27
10	0.30	1.16	4.00	0.89	1.20	0.23	0.99	3.71
	0.35	1.31	4.74	0.99	1.24	0.34	1.11	4.49

[a]Nominal electronic reflection symmetry of final states (see Ref. 21).

in the Appendix, are expressed not in terms of $V_{A'}$ and $V_{A''}$ directly, but in terms of the average and one-half the difference of these potentials.[3] Because the A' and A'' PESs are so qualitatively different (see Fig. 1), the difference potential for ArCH(X) is large. In fact, the difference potential is dominated by just one term, the lowest order anisotropy $V_{22}(R)$, which is comparable in magnitude to the largest anisotropy in the expansion of the average potential $V_{20}(R)$.

Cross sections for rotationally inelastic collisions of CH($X\ ^2\Pi$) with Ar were determined with our HIBRIDON code.[47] All energetically open, and at least one closed, rotational levels were included in the channel basis. We used the spectroscopic constants of Bernath *et al.*[34] for the calculation of the asymptotic CH($X\ ^2\Pi$) rotational energies [and hence the wave vectors in Eq. (5)] in the $v=0$ vibrational level.

The calculated cross sections for high-N initial states are found to be appreciable only for $\Delta N=0$ and for $\Delta N=-1$ fine-structure conserving ($F_i\rightarrow F_i$) transitions. For high initial N the small cross sections for downward transitions with changes of $\Delta N>1$ are the result of the large energy gaps (comparable to or larger than the incident translational energy). For example, the $\Delta N=-1$ and -2 energy gaps are 426 and 824 cm^{-1}, respectively, for initial $N=15$. At translational energies comparable to kT, upward transitions are energetically forbidden for such high initial N. This implies that the collisional relaxation of highly rotationally excited CH($X\ ^2\Pi$) proceeds, at least in the early stages, by successive $\Delta N=-1$ transitions to the next lower rotational manifold, with concomitant collisional transitions within the fine-structure sublevels associated with a given rotational level.

As an alternative to full CC calculations, a significant reduction in the dimensionality and consequent decrease in computer time can be achieved within the CD approximation, in which the CC equations are partitioned into noninteracting blocks corresponding to different values of P, the body frame projection of J. A comparison of calculated CC and CD cross sections for $\Delta N=-1$ fine-structure conserving transitions out of $N=8$ and $N=10$ is shown in Table I. We observe that the error in the CD cross sections is less than 15% and, further, that CD calculations correctly predict the relative magnitudes of the fine-structure resolved cross sections for a given $F_i\rightarrow F_i$ transition. Accordingly, for computational ease, the CD approximation was used for the determination of the remainder of the cross sections reported here.

Table II presents calculated CH($X\ ^2\Pi$)–Ar cross sections for $\Delta N=-1$ fine-structure conserving and changing transitions for representative values of initial N at an incident translational energy of 300 cm^{-1}. At low initial N the cross sections for transitions in which the fine-structure label changes are comparable to those for transitions in which this label is unchanged. However, at high initial N there appears a clear propensity for conservation of the fine-structure label. We explained this previously by means of a formal quantum analysis of the collision dynamics[2]: Under the influence of purely electrostatic interactions a collision can affect the magnitude and orientation of the rotational angular momentum **N** but not that of the electron spin **S**. Furthermore, most collisions are glancing encounters and hence effect only small changes in the magnitude and direction of N. Thus the relative orientation of **N** and **S**, which is reflected in the F_i label, will have a tendency to remain unchanged in the collision.

We also see from Table II that for low initial N the largest cross sections for fine-structure conserving transitions involve a change of the e/f label, and that the cross sections into final $\Pi(A')$ levels are slightly larger than those into $\Pi(A'')$ levels, as discussed and explained previously by Dagdigian *et al.*[18] By contrast, for high initial N the latter propensity is *reversed*, so that the largest fine-structure conserving cross sections are those for $\Pi(A')\rightarrow\Pi(A'')$ transitions. Since, as discussed in the preceding paragraph, the large cross sections occur for transitions in which the F_i label is conserved, the two dominant $N\rightarrow N-1$ transitions are $F_1e\rightarrow F_1f$ and $F_2f\rightarrow F_2e$.

We can obtain a quantitative measure of the tendency to populate preferentially levels of $\Pi(A')$ or $\Pi(A'')$ reflection symmetry by defining the *Λ-doublet polarization* of the $N\rightarrow N-1$ inelastic cross sections, namely

$$P_{N\rightarrow N-1}(F_i)=[\sigma_{\Pi(A'')}-\sigma_{\Pi(A')}]/[\sigma_{\Pi(A'')}+\sigma_{\Pi(A')}], \tag{13}$$

where $\sigma_{\Pi(A'')}$ designates the *sum* of the two cross sections for population of levels of $\Pi(A'')$ symmetry ($F_1e\rightarrow F_1f$ and $F_1f\rightarrow F_1f$, for the F_1 manifold) and similarly for $\sigma_{\Pi(A')}$. This polarization would attain a value of unity in the limit where collisions would populate $\Pi(A'')$ levels exclusively. These Λ-doublet polarizations, for transitions out of both the F_1 and F_2 manifolds, are plotted in Fig. 2 as a function of N. This polarization is seen to increase monotonically, which

TABLE II. Calculated CH($X\ ^2\Pi$)–Ar cross sections (in Å^2) for $\Delta N=-1$ transitions at an incident translational energy of 300 cm^{-1}.

Initial N	$e\rightarrow e$	$f\rightarrow f$	$e\rightarrow f$	$f\rightarrow e$	$e\rightarrow e$	$f\rightarrow f$	$e\rightarrow f$	$f\rightarrow e$
	$F_1\rightarrow F_1$				$F_2\rightarrow F_2$			
	$\Pi(A')$[a]	$\Pi(A'')$	$\Pi(A'')$	$\Pi(A')$	$\Pi(A'')$	$\Pi(A')$	$\Pi(A')$	$\Pi(A'')$
2	0.16	0.13	1.81	3.18	0.03	0.02	1.70	1.49
3	0.25	0.19	2.81	2.08	0.18	0.13	1.84	1.91
4	0.45	0.89	4.00	0.92	0.62	0.26	0.91	3.18
5	0.79	1.20	5.40	1.72	1.03	0.61	1.66	4.42
8	0.57	1.82	5.08	1.28	1.66	0.53	1.40	4.75
11	0.20	0.89	3.61	0.71	0.93	0.20	0.80	3.39
14	0.06	0.31	2.80	0.33	0.32	0.06	0.37	2.71
17	0.01	0.01	2.24	0.03	0.09	0.02	0.15	2.23
	$F_1\rightarrow F_2$				$F_2\rightarrow F_1$			
	$\Pi(A'')$[a]	$\Pi(A')$	$\Pi(A')$	$\Pi(A'')$	$\Pi(A')$	$\Pi(A'')$	$\Pi(A'')$	$\Pi(A')$
2	0.43	0.67	0.06	0.11	0.52	2.00	0.27	0.19
3	0.88	0.59	0.14	0.11	0.75	2.37	0.22	0.29
4	1.06	0.66	0.26	0.17	0.98	2.25	0.29	0.46
5	1.27	0.44	0.22	0.63	0.54	2.38	0.89	0.32
8	0.53	0.36	0.03	0.60	0.33	1.63	0.81	0.04
11	0.33	0.11	0.005	0.09	0.10	1.10	0.10	0.008
14	0.21	0.03	0.001	0.013	0.03	0.71	0.016	0.002
17	0.11	0.002	0.0002	0.001	0.005	0.39	0.003	0.001

[a]Nominal electronic reflection symmetry of final states (see Ref. 21).

reveals that as N increases, inelastic collisions increasingly select only final states of $\Pi(A'')$ reflection symmetry.

The summed inelastic cross section for a given $N\rightarrow N-1$ transition is given by summing those cross sections listed in Table II over all possible final, and averaging over all initial, fine-structure and Λ-doublet levels. These summed cross sections are shown in Fig. 3. We observe that for $N\geqslant 8$ these summed cross sections decrease with increasing N. This behavior reflects the fact that as the energy gap for the $N\rightarrow N-1$ transition increases, the transition becomes less facile, for a given initial translational energy.

From the cross sections presented in Tables I and II one can understand qualitatively the observations by Hancock, Stuhl, and their co-workers[24,25] of the production of preferential populations in $\Pi(A'')$ Λ-doublet levels in the collisional relaxation of CH($X\ ^2\Pi$) by Ar. The total removal cross sections for high initial N by all $\Delta N=-1$ transitions is (see Table II) much larger out of $\Pi(A')$ levels [F_1e and F_2f] than out of $\Pi(A'')$ levels [F_1f and F_2e]. This implies that the $\Pi(A')$ levels will be relaxed by collisions more efficiently than the $\Pi(A'')$ levels. Moreover, as shown by Table II, the largest of these $\Delta N=-1$ cross sections involve transitions *into* levels of $\Pi(A'')$ symmetry. Thus, the populations of $\Pi(A'')$ levels will be enhanced relative to those of the $\Pi(A')$ levels by both the preferential depletion of $\Pi(A')$ levels *and* the preferential formation of $\Pi(A'')$ levels in lower N manifolds.

In principle, this population imbalance could be counteracted by $\Delta N=0$ transitions which would transfer population between $\Pi(A')$ and $\Pi(A'')$ levels of the same N. Table III presents calculated CH($X\ ^2\Pi$)–Ar cross sections for $\Delta N=0$ transitions for representative values of initial N at an incident translational energy of 300 cm^{-1}. For low initial N the larg-

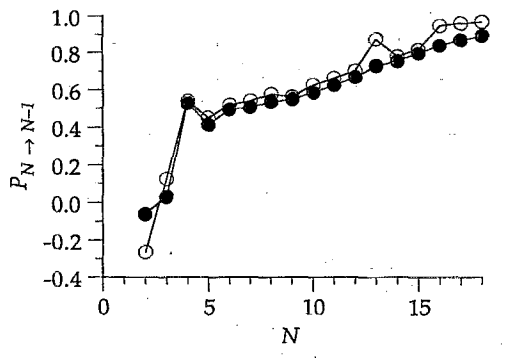

FIG. 2. The Λ-doublet polarization [defined by Eq. (13)] of the fine-structure conserving inelastic CH(X)–Ar $N\rightarrow N-1$ cross sections as a function of the rotational quantum number N. The open and filled circles designate, respectively, the $F_1\rightarrow F_1$ and $F_2\rightarrow F_2$ transitions.

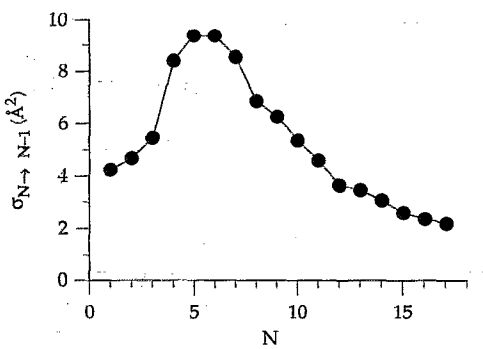

FIG. 3. Inelastic CH(X)–Ar $N\rightarrow N-1$ cross sections, summed over the final state and averaged over the initial state fine-structure and Λ-doublet levels.

TABLE III. Calculated CH($X\ ^2\Pi$)–Ar cross sections (in Å^2) for $\Delta N=0$ transitions at an incident translational energy of 300 cm^{-1}.

Initial N	$e\rightarrow f$	$f\rightarrow e$	$e\rightarrow e$	$f\rightarrow f$	$e\rightarrow f$	$f\rightarrow e$
	$F_1\rightarrow F_1$		$F_1\rightarrow F_2$			
	$\Pi(A'')$[a]	$\Pi(A')$	$\Pi(A'')$	$\Pi(A')$	$\Pi(A')$	$\Pi(A'')$
2	0.15	0.15	0.06	0.03	3.35	1.79
5	0.61	0.61	0.20	0.27	2.52	6.51
8	1.24	1.22	0.17	0.23	2.53	2.62
11	0.92	0.90	0.06	0.09	2.14	1.27
14	0.66	0.64	0.03	0.04	1.73	0.67
17	0.56	0.54	0.02	0.02	1.35	0.38
	$F_2\rightarrow F_2$		$F_2\rightarrow F_1$			
	$\Pi(A')$	$\Pi(A'')$	$\Pi(A')$	$\Pi(A'')$	$\Pi(A'')$	$\Pi(A')$
2	0.17	0.17	0.09	0.04	2.63	4.93
5	0.67	0.67	0.24	0.33	7.75	3.00
8	1.43	1.45	0.19	0.26	2.93	2.83
11	1.06	1.08	0.07	0.10	1.38	2.33
14	0.73	0.75	0.03	0.04	0.71	1.85
17	0.51	0.53	0.01	0.02	0.40	1.43

[a]Nominal electronic reflection symmetry of final states (see Ref. 21).

est cross sections involve $F_1\leftrightarrow F_2$ transitions with a change of the *e/f* label, and the cross sections into final $\Pi(A')$ levels are slightly larger than those into $\Pi(A'')$ levels. For high initial N the former propensity becomes more pronounced: the two dominant $\Delta N=0$ cross sections [$F_1e\rightarrow F_2f$ and $F_2f\rightarrow F_1e$] are for the two $\Pi(A')\rightarrow\Pi(A')$ $F_1\leftrightarrow F_2$ transitions. Thus, the $\Delta N=0$ transitions with the largest cross sections will *conserve* the approximate reflection symmetry and hence *not* counteract the enhancement of the population in the $\Pi(A'')$ levels due to the $\Delta N=-1$ transitions.

IV. EXPLANATION OF OBSERVED Λ-DOUBLET PROPENSITY

In our previous investigation[18] of the inelastic scattering of $^2\Pi$ [case (b)] molecules, we were able to rationalize the Λ-doublet propensities manifest in the calculated CH($X\ ^2\Pi$)–Ar cross sections involving low initial N by consideration of the magnitude of the direct coupling between the initial and final states. We have been unable to use a similar type of argument to explain the dramatic propensities which accompany relaxation of levels with high initial N. Rather, we present here a simple physical argument based on consideration of the rotational motion of the CH moiety at high initial N.

Consider two limiting cases, as shown schematically in Fig. 4. In the first the CH molecule approaches the Ar atom rotating so that **J** is perpendicular to **R**. In this "pinwheel" motion the projection of **J** along **R**, denoted here by P, attains its smallest magnitude: $|P|=0.5$. If the CH–Ar approach is slow compared to the rotational motion then, in this limiting case, we see from Fig. 4 that the encounter will be governed by the average, over θ, of the interaction potential. In particular, for encounters involving CH in a $\Pi(A')$ Λ-doublet level, in which the singly filled π orbital lies in the plane of rotation of the molecule (in the high-N limit),[21] the effective potential will be the average, over θ, of the $V_{A'}$ PES, while, for encounters involving CH in a $\Pi(A'')$ Λ-doublet level, the effective potential will be the average of the $V_{A''}$ PES.

In the second limiting case the CH molecule approaches the Ar atom rotating so that **J** is parallel to **R**. In this "helicopter" motion the projection of **J** along **R** attains its largest possible magnitude: $|P|=J$. If the CH–Ar approach is slow compared to the rotational motion then, in this limiting case, we see from Fig. 4 that the encounter will be governed by $V(R,\theta=90°)$. In particular, for encounters involving CH in

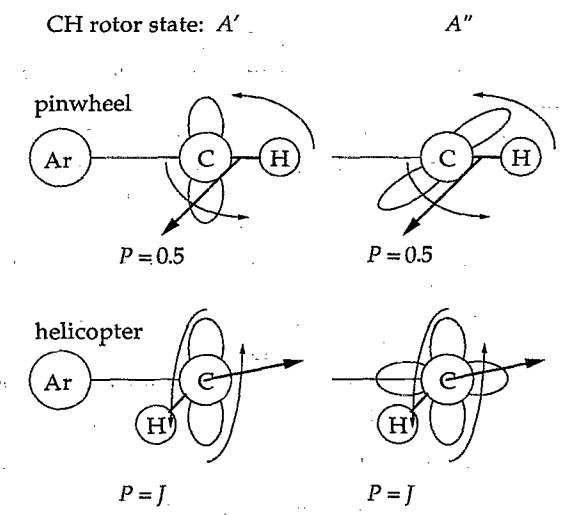

FIG. 4. Schematic cartoon describing approach of a rotating CH molecule to an Ar atom. When the CH molecule approaches so that its rotational angular momentum **J** (designated here by the heavy arrow) is perpendicular to **R** (pinwheel motion), the effective potential experienced will be the *average* over the Jacobi angle θ of the A' or A'' PESs. When, however, the CH molecule approaches so that its rotational angular momentum **J** is parallel to **R** (helicopter motion), the effective potential experienced will be, respectively, the A'' or A' PESs (note the *reversal*) evaluated at $\theta=90°$.

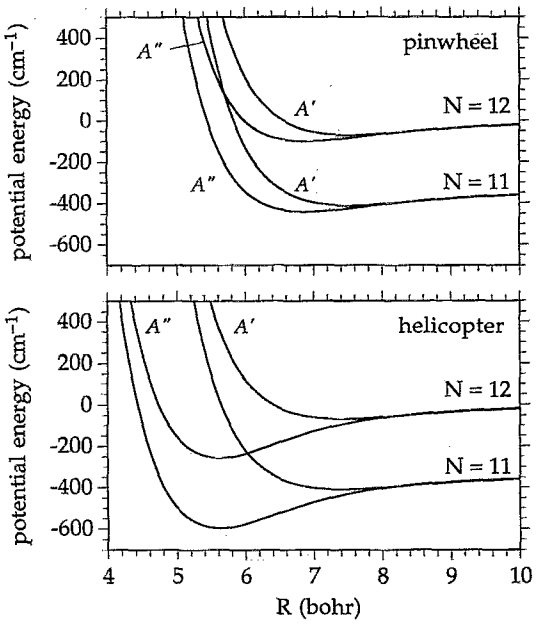

FIG. 5. (Upper panel) plot of the *average* over the Jacobi angle θ of the A' or A'' PESs. In the high-J limit this is the effective potential experienced by the CH molecule during the pinwheel approach during which **J** lies perpendicular to **R**. Shown are two sets of curves which correlate, asymptotically, with the $N=11$ and $N=12$ rotational levels of the CH(X) molecule. (Lower panel) similar plot but of the A' and A'' PESs evaluated at $\theta=90°$. In the high-J limit this is the effective potential experienced by the CH molecule during the helicopter approach during which **J** lies parallel to **R**.

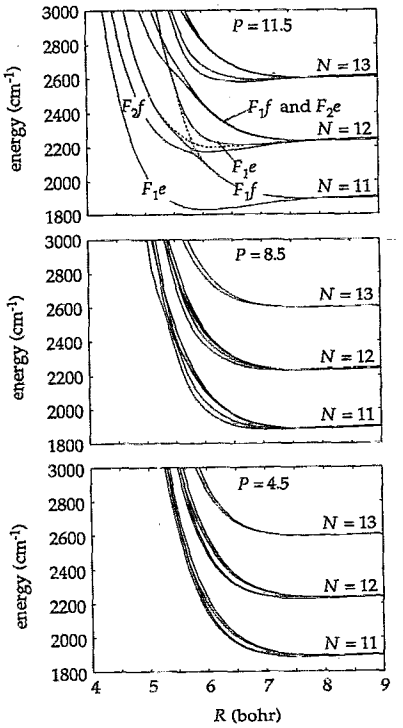

FIG. 6. Plots of the adiabatic bender potentials for the ArCH(X) system within the centrifugal decoupling approximation for three values of the body frame projection quantum number P and a total angular momentum $\bar{L}=30$ (this value is representative of those for which the partial cross sections are largest; see Fig. 7). Shown are all the adiabatic bender potentials which correlate with the $N=11$, 12, and 13 multiplet levels of the CH(X) molecule. For $P=11.5$ (top panel), only the F_1 states ($J=N+1/2$) exist for $N=11$. For $P=11.5$ the avoided crossing between the $N=12$, $F_1e[\Pi(A')]$ and the $N=11$, $F_1f[\Pi(A'')]$ states is seen clearly; the underlying diabatic potentials are indicated schematically by dashed lines. This crossing provides the dominant mechanism for $N\rightarrow N-1$ rotational relaxation. Only a hint of this avoided crossing is seen at $P=8.5$, and none whatsoever for $P=4.5$.

a $\Pi(A')$ Λ-doublet level the effective potential will be $V_{A''}(R,\theta=90°)$, while, for encounters involving CH in a $\Pi(A'')$ Λ-doublet level, the effective potential will be $V_{A'}(R,\theta=90°)$.

Figure 5 illustrates the dependence on R of the effective potentials for pinwheel and helicopter approach. We observe that for helicopter-like orientation, a CH molecule in the $\Pi(A')$ Λ-doublet level can approach the Ar atom on the attractive A'' PES and then cross over to the repulsive A' PES correlating with the next lower rotational asymptote. Although a crossing is also present for the pinwheel approach, it occurs at higher energy, and at a shorter CH–Ar distance.

To render these ideas more quantitative, we plot in Fig. 6 radial "adiabatic bender" potentials[28] for low ($P=0.5$) and high ($P=J$) values of the BF projection quantum number. These potentials are defined by

$$w_{\rm ad}(R)=T_P(R)W_P(R)T_P^T(R), \tag{14}$$

where $T_P(R)$ is the matrix which diagonalizes the $W_P(R)$ subblock of the $W(R)$ matrix at each value of R. In previous work, we, and others, have demonstrated the pedagogical use of adiabatic potentials in the analysis of both rotationally inelastic molecular collisions[13,48] and the related study of bound bend–stretch levels of weakly bound complexes.[28,40,49]

Figure 6 displays the ArCH(X) adiabatic bender potentials which correlate with the $N=11$, 12, and 13 rotational levels of the isolated CH(X) molecule for $P=4.5$, 8.5, and 11.5. We observe that at the highest value of P the adiabatic bender potentials are qualitatively similar to the potentials for the helicopter approach seen in the lower panel of Fig. 5. We observe a strong avoided crossing between the $N=12$, F_1e adiabat, which corresponds to a state of A' symmetry, and the $N=11$, F_1f adiabat, which corresponds to a state of A'' symmetry. For the pinwheel approach, however, the adiabatic curves, which include the full interaction potential, not just the diagonal coupling shown in Fig. 5, reveal no evidence of any significant curve crossing which would couple the fine-structure multiplets associated with two different rotational levels.

In principle this crossing provides a pathway for rotational relaxation, even though the $N=12\rightarrow 11$ energy gap is large ($\cong$340 cm^{-1}). The approach of CH molecules in a $\Pi(A')$ Λ-doublet level with $P=J$ will be governed, as shown schematically in Figs. 4 and 5, by the $\theta=90°$ cut in the A'' PES. As we discussed in Sec. III above, the A'' PES is most attractive in perpendicular geometry, with a deep well located at $R\cong 5.7$ bohr. As the CH molecule approaches along this adiabat, it transits through a region of strong

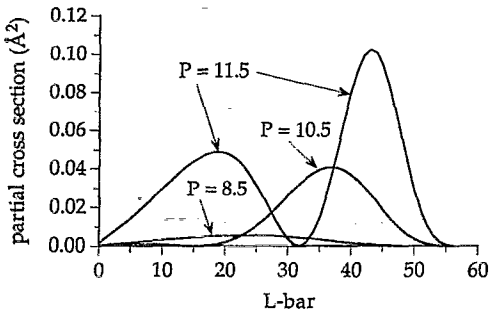

FIG. 7. Partial cross sections [Eq. (12)] for the $N=12$, $F_1e \rightarrow N=11$, F_1f as a function of the CD partial wave index, for three values of the projection quantum number P.

avoided crossing with the adiabat associated with the $\Pi(A')$ Λ-doublet level associated with the next lower N (here $N=11$). As shown schematically in Figs. 4 and 5, the approach of CH molecules in an A'' Λ-doublet level with $P \cong J$ will be governed by the perpendicular orientation of the A' PES, which does not have an attractive well and where the onset of the repulsive wall occurs at larger values of R.

This mechanism, involving passage from the attractive adiabat which correlates with the rotational level N to the repulsive adiabat which correlates with the next lower rotational level, was invoked originally by Lebed *et al.*[29] in a paper focused on the mechanism of the rotational relaxation in the $B\ ^1\Pi_u$ state of the akali dimers. In that paper, from the qualitative form of the π orbital, these authors derived a figure (see Fig. 2 of Ref. 29) essentially equivalent to our Fig. 5. In a similar manner, the observed rapid collisional vibrational relaxation of $NCO(\tilde{X}\ ^2\Pi)$ in its ν_2 bending mode has been explained by the crossing of attractive and repulsive PESs emanating from successive bending vibrational levels.[50]

We observe in Fig. 6 that the avoided crossing is much less apparent for lower values of the BF projection quantum number. Thus we anticipate that collision induced $N \rightarrow N-1$ transitions will occur primarily during helicopter-like encounters. To demonstrate this we show in Fig. 7 the partial cross sections, within the CD approximation [see Eq. (12)], for the $N=12$, $F_1e \rightarrow N=11$, F_1f transition, which, as we see from Table II, is that dominant pathway for relaxation of the $N=12$, F_1 Λ doublet. As anticipated, the partial cross section is largest when P equals the maximum allowable value in the final state ($P=11.5$) and significant only for the highest two or three possible values of P.

We further observe in Fig. 7 a marked oscillatory structure in the dominant partial cross section ($P=11.5$). This is likely a manifestation of quantum interference, similar to Stückelberg oscillations.[51] In a semiclassical description the $N=12 \rightarrow 11$ transition can occur by curve crossing (illustrated in the upper panel of Fig. 6) as Ar approaches and as it recedes.

As a further demonstration that the efficient $N \rightarrow N-1$ relaxation of the high-N levels of the $CH(X)$ molecule involves a crossing between two adiabatic bender potentials which follow, respectively, the A' and A'' PES, we present in Table IV cross sections calculated with several simplified choices of the PESs, all of which involved replacing both the A' and A'' PESs with a *single* PES. Because only a single PES was used, the difference potential was identically zero. For the single PES we used (a) the A' PES, (b) the A'' PES, and (c) the average of $V_{A'}$ and $V_{A''}$. Table IV compares the predicted cross sections for transitions from $N=15$ to $N=14$. We observe that the calculated cross sections for the $N=15$ $\Pi(A') \rightarrow N=14$ $\Pi(A'')$ transition is far smaller, by at least a factor of 100, than when both PESs are simultaneously present. As anticipated, this is further confirmation that it is the avoided crossing between two adiabatic bender potentials which facilitates the efficient $N \rightarrow N-1$ relaxation.

V. KINETIC SIMULATION OF THE COLLISIONAL RELAXATION OF CH($X\ ^2\Pi$) BY ARGON

The above analysis provides a qualitative rationalization of the observed[24,25] preferential population of $\Pi(A'')$ levels in the collisional relaxation of $CH(X\ ^2\Pi)$ by Ar. To predict the magnitude of the enhancement of the $\Pi(A'')$ populations, we have carried out a kinetic simulation of the collisional relaxation of the nascent $CH(X\ ^2\Pi)$ fragments from the two-photon dissociation of ketene in order to model the observations of Hancock and co-workers.[24] All spin–orbit and Λ-doublet levels with $N \leqslant 18$ were included (a total of 72 rotational/fine-structure levels). For each initial N manifold,

TABLE IV. Dependence on the potential energy surface of $CH(X\ ^2\Pi)$–Ar cross sections (in Å²) for $N=15 \rightarrow N=14$ transitions at an incident translational energy of 300 cm^{-1}.

$F_1 \rightarrow F_1$				$F_2 \rightarrow F_2$			
$e \rightarrow e$	$f \rightarrow f$	$e \rightarrow f$	$f \rightarrow e$	$e \rightarrow e$	$f \rightarrow f$	$e \rightarrow f$	$f \rightarrow e$
$\Pi(A')$[a]	$\Pi(A'')$	$\Pi(A'')$	$\Pi(A')$	$\Pi(A'')$	$\Pi(A')$	$\Pi(A')$	$\Pi(A'')$
			ab initio potential				
0.036	0.233	2.59	0.246	0.210	0.038	0.271	2.54
			$V=V_{av}:V_{dif}=0$				
0.075	0.083	0.008	0.011	0.082	0.074	0.012	0.001
			$V=V_{A'}:V_{dif}=0$				
0.027	0.029	0.002	0.003	0.041	0.037	0.004	0.003
			$V=V_{A'}:V_{dif}=0$				
0.150	0.163	0.025	0.029	0.131	0.121	0.027	0.023

[a]Nominal electronic reflection symmetry of final states (see Ref. 21).

downward ($\Delta N \leqslant 0$) state-to-state rate constants for collisions of CH($X\ ^2\Pi$) with Ar were obtained as follows: The calculated downward ($N' \leqslant N$) CS cross sections, computed for an incident kinetic energy of 300 cm^{-1} ($\approx \frac{3}{2}$ kT), were converted to bimolecular rate constants through multiplication by the average CH–Ar relative velocity at room temperature (8.04×10^4 cm s^{-1}), namely

$$k_{i\to f}(T) = \int \sigma_{i\to f}(v) v f(v) dv \cong \sigma_{i\to f}(v_{mp}) v_{mp}, \quad (15)$$

where $f(v)$ is a Maxwellian velocity distribution. The rate constants for upward ($N' > N$) transitions were determined by microscopic reversibility.

We then integrated numerically[52] the master equation describing the time evolution of the populations. For the initial populations we used the nascent CH($X\ ^2\Pi$) rotational state distribution determined by Ball *et al.*[23] in the two-photon dissociation of ketene at 279.3 nm. Because of spectral overlap, the nascent spin–orbit state distribution could not be determined in this experiment. Consequently, we assumed equal initial spin–orbit populations. We also took equal initial populations in both Λ-doublet levels, as was seen experimentally by Ball *et al.*[23] In some simulations, we included removal of CH by reaction with ketene. In this latter case, the room temperature rate constant determined by Hancock and Heal[53] (2.4×10^{-10} cm^3 $molecule^{-1}$ s^{-1}) was employed; we assumed that this removal rate constant was identical for all CH($X\ ^2\Pi$) levels and, further, independent of the initial Λ-doublet level.

In our simulations, we have focused mainly on the time evolution of the $N=15$ rotational populations, whose collisional relaxation was experimentally investigated in detail by Ball *et al.*[24] The two panels of Fig. 8 compare the computed time-dependent populations of the $\Pi(A'')$ and $\Pi(A')$ Λ-doublet levels for $N=15$ without and with the inclusion of removal of CH($X\ ^2\Pi$) by reaction with ketene. It can be seen that, in both cases, the $\Pi(A')$ population has an initial rapid drop, while the $\Pi(A'')$ population initially increases. As noted at the end of Sec. III, the former reflects the larger depletion rate out of $\Pi(A')$ vs $\Pi(A'')$ levels, while the latter is a result of the selective production of $\Pi(A'')$ in $\Delta N = -1$ collisional transitions.

We also see from Fig. 8 that the $N=15$ populations drop much more rapidly when the removal of CH($X\ ^2\Pi$) through reaction with ketene is included in the kinetic simulation. In fact, the time-dependent populations computed with inclusion of this reaction mirror quite closely the experimentally measured time-dependent $N=15$ populations presented by Ball *et al.*[24] This comparison indicates that reaction with ketene is, in fact, the dominant CH($X\ ^2\Pi$) collisional removal mechanism under the conditions of their experiment, as Ball *et al.* have stated.

Ball *et al.*[24] have also monitored the time dependence of the ratio of the $N=15$ $\Pi(A'')$ and $\Pi(A')$ populations and find that this ratio increases with time from the nascent value of unity to a value of approximately 1.7. They find that this ratio remains roughly constant even though the total population in $N=15$ is decreasing with time. With 0.5 Torr of argon, the asymptotic Λ-doublet ratio is reached in approximately 5 μs. While quantitative measurements of the Λ-doublet ratios were not reported by Ball *et al.*[24] for lower N levels, they remark that preferential Λ-doublet populations are not observed for rotational levels with $N \leqslant 12$.

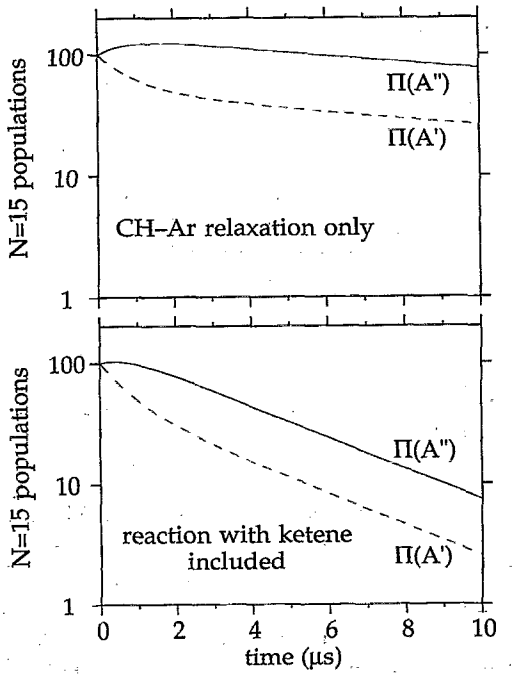

FIG. 8. Semilogarithmic plots of the time-dependent populations of the $N=15$ $\Pi(A'')$ (solid lines) and $\Pi(A')$ (dashed lines) Λ-doublet levels (summed over the fine-structure levels) computed from kinetic simulations without (top panel) and with (bottom panel) the inclusion of removal of CH($X\ ^2\Pi$) by reaction with ketene. The initial CH($X\ ^2\Pi$) rotational state distribution was taken as that appropriate to the nascent distribution in the 279.3 nm two-photon photolysis of ketene (Ref. 23). The partial pressures of argon and ketene were taken to be 1 Torr and 30 mTorr, respectively. The rotational state populations have been normalized so that the population for $N=15$ equals 100 for zero time.

Figure 9 presents calculated Λ-doublet ratios as a func-

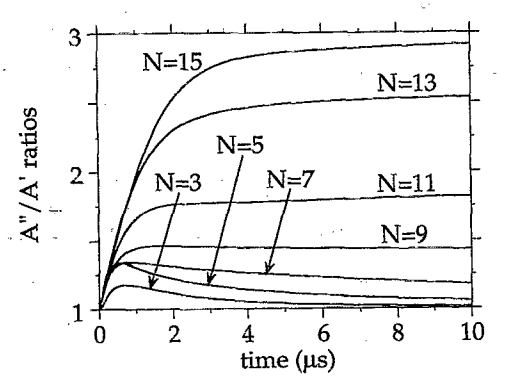

FIG. 9. Time dependence of ratios of $\Pi(A'')$ to $\Pi(A')$ Λ-doublet populations (summed over the fine-structure levels) for various N levels computed from a kinetic simulation using our calculated Ar–CH($X\ ^2\Pi$) rotationally inelastic cross sections and including removal of CH($X\ ^2\Pi$) by reaction with ketene. The initial CH($X\ ^2\Pi$) rotational state distribution was taken as that appropriate to the nascent distribution in the 279.3 nm two-photon photolysis of ketene (Ref. 23). The partial pressures of argon and ketene were taken to be 1 Torr and 30 mTorr, respectively.

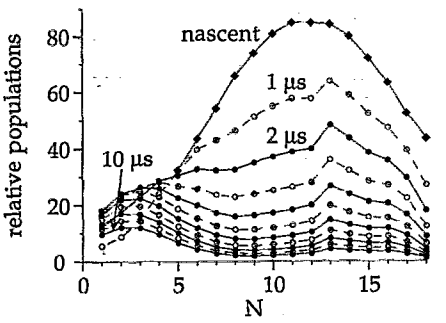

FIG. 10. Rotational level distributions (summed over the fine-structure and Λ-doublet levels) as a function of N calculated from a kinetic simulation of the collisional relaxation of CH($X\ ^2\Pi$) for various times (1 to 10 μs, in increments of 1 μs). The initial CH($X\ ^2\Pi$) rotational state distribution (diamonds) was taken as that appropriate to the nascent distribution in the 279.3 nm two-photon photolysis of ketene (Ref. 23). The partial pressures of argon and ketene were taken to be 1 Torr and 30 mTorr, respectively. The kinetic simulation employed our calculated Ar–CH($X\ ^2\Pi$) rotationally inelastic cross sections and included removal of CH($X\ ^2\Pi$) by reaction with ketene. The rotational state populations have been normalized so that the nascent CH distribution summed over all levels equals 1000.

tion of time for a range of N levels. In this kinetic simulation, removal by reaction with ketene was included. However, the calculated Λ-doublet ratios were found to be virtually identical if this removal process were not included in the input cross sections, although in this case the rotational populations for high N did not decay as fast, as can be seen from Fig. 4 for $N=15$. For all values of N, we found an enhancement of the $\Pi(A'')$ populations over those for the $\Pi(A')$ levels. After an induction period, which was larger for higher N, the Λ-doublet ratios reached asymptotic, time-independent values.

The asymptotic $\Pi(A'')$ to $\Pi(A')$ Λ-doublet population ratios increased strongly with increasing N, reaching a value of 2.9 for $N=15$, the highest level shown in Fig. 9. This asymptotic Λ-doublet ratio for $N=15$ is larger than that measured by Ball *et al.*[24] However, our kinetic simulation reproduces reasonably well their observed time dependence of this ratio. We find for $N=15$ (see Fig. 9) that the asymptotic ratio is reached in a pressure-time product of 3 Torr μs, while Ball *et al.*[24] find that a time-pressure product of ~2.5 Torr μs is required to reach the limiting ratio. The Λ-doublet ratios presented in Fig. 9 also reproduce the qualitative dependence in the Λ-doublet ratios noted by Ball *et al.*[24] for the lower N levels. These comparisons indicate that, while our kinetic simulation has not quantitatively reproduced the observed $N=15$ $\Pi(A'')$ to $\Pi(A')$ population ratio, the simulation is sufficiently accurate to explain the qualitative features observed by Ball *et al.*[24] in the collisional relaxation of CH($X\ ^2\Pi$) by argon.

Figure 10 displays the calculated rotational level population distribution (summed over fine-structure and Λ-doublet levels) as a function of N for various times. It can be seen that after several μs (at 1 Torr total pressure) the distribution becomes bimodal, with a room temperature thermalized low-N portion and a remnant of the nascent distribution at high N. For the latter, the relative populations of successive $N,N-1$ manifolds remain approximately constant, as observed experimentally.[24] The total concentration of CH($X\ ^2\Pi$) is dropping with increasing time because of the inclusion of reaction with ketene in the simulation.

Heinrich and Stuhl[25] have also measured the time dependence of the $\Pi(A'')$ to $\Pi(A')$ Λ-doublet population ratio for $N=15$ in the collisional relaxation by Ar of CH($X\ ^2\Pi$) radicals formed in the 193 nm photolysis of CH_2Br_2. At 0.35 Torr total pressure, they found that this ratio reached the asymptotic valus of approximately 3. This value is in good agreement with the results of our kinetic simulation. They observe that this asymptotic ratio is reached within a pressure-time product of 4–5 Torr μs, in reasonable agreement with our kinetic simulations.

VI. CONCLUSIONS

In this paper we present calculated CH($X\ ^2\Pi$)–Ar rotationally inelastic cross sections, determined using our modified *ab initio* PESs.[27] Our primary focus here was the relaxation of high rotational levels of CH($X\ ^2\Pi$). With the calculated cross sections we were able to understand qualitatively, and, by means of kinetic simulations, reproduce quantitatively the experimental observations[24,25] of the appearance of preferential $\Pi(A'')$ Λ-doublet populations during the relaxation of an initial rotational state distribution with no initial Λ-doublet state specificity.

For relaxation of high-N levels, the largest cross sections were associated with transitions in which the relative orientation of **N** and **S** is conserved during the collision (F_i conserving) and in which a $\Pi(A')$ level (F_1e or F_2f) relaxes to a $\Pi(A'')$ level (F_1f or F_2e) in the next lower $(N-1)$ rotational multiplet. Thus, the origin of the observed Λ-doublet preferences involves both the enhanced *depletion* of high-N $\Pi(A')$ levels and the enhanced *formation* of $\Pi(A'')$ levels in the next lower $(N-1)$ manifold. Physically, the observed propensity is a result of a crossing between the more attractive PES ($V_{A''}$) which correlates with the higher (N) rotational asymptote and the less attractive PES ($V_{A'}$) which correlates with the lower $(N-1)$ rotational asymptote. This is a concrete example of a mechanism proposed some years ago by Nikitin and co-workers, for collisions involving molecules in $^1\Pi$ electronic states.[29] The crossing depends crucially on the orientation of the rotational angular momentum of the incoming CH molecule with respect to the initial direction of approach (a v, N correlation), since a significant crossing occurs only for the helicopter-like approach ($\mathbf{v}\|N$). In fact, what Hancock, Stuhl, and their co-workers have observed is a strong v, N correlation in the reactant channel which gives rise to a strong Λ', N' correlation in the product channel.

The observed propensity, although well predicted by our calculations and understood in terms of the curve crossing model discussed in the preceding paragraph, is opposite to the observed[20] propensity for collisional transitions between *low* rotational levels of CH(X). This later propensity is a direct manifestation of the relative strength of the potential matrix elements which couple the various initial and final states in question.[18] In the present case, involving relaxation of high-N levels, the observed Λ-doublet propensity is a manifestation not of the relative strength of various *off-*

diagonal coupling matrix elements, but of the behavior of the *diagonal* matrix elements of the interaction potential, which allow a crossing between two adiabatic states which correlate with different rotational asymptotes. Nonetheless, in both cases (low and high N) the Λ-doublet propensities result from quantum interference between collisions which sample both the A' and A'' PES.

We conclude from this comparison between the relaxation of low- and high-N levels that one must exercise great care in using simplistic models to make global predictions about the preferential populations of Λ-doublet levels in collision-induced rotational transitions of open-shell molecules. In some recent studies of molecular photodissociation,[54] observation of unequal Λ-doublet populations in the photofragments is often used as a clue to the photofragmentation mechanism.[55] The observations of Hancock, Stuhl, Reisler, and their co-workers[24–26] imply that Λ-doublet asymmetries can result both from the photofragmentation as well as from subsequent collisional relaxation of the photofragments.

In the case considered here, namely the relaxation of $CH(X\ ^2\Pi)$ in collision with Ar, the A' and A'' PES differ most significantly in T-shaped geometry, where the A'' PES has a deep well. The relaxation of high-N levels, and the observed Λ-doublet propensity, are direct manifestations of this difference in the topology of the two PESs. For other diatomic radicals in Π electronic states, the topology of the A' and A'' PESs can be quite different. In such cases, the relaxation of high-J levels may well be less (or more) efficient than the case of Ar–CH(X), and the Λ-doublet propensities may be quite different. We anticipate that future experimental work will continue to challenge our ability to understand the mechanism of rotational relaxation in other open-shell systems.

ACKNOWLEDGMENTS

We would like to acknowledge gratefully G. Hancock, whose conversations about the experiments reported in Ref. 24 stimulated our interest in this topic. We also thank F. Stuhl and H. Reisler for communicating to us unpublished results from their laboratories, and A. Berning for helpful comments on the original manuscript. This research has been supported by the National Science Foundation under Grant No. CHE-9223081 and by the U. S. Army Research Office under Grant No. DAAL-03-91-G-0123.

APPENDIX

In the full SF intermediate coupling basis, the matrix elements of the interaction potential can be written as[15,18]

$$\langle J'F_i'\epsilon'L'\mathscr{J}\mathscr{M}|V|JF_i\epsilon L\mathscr{J}\mathscr{M}\rangle = (-1)^{\mathscr{J}+J+J'-1/2}[(2L+1)(2L'+1)(2J+1)(2J'+1)]^{1/2}\sum_l \begin{pmatrix} L' & l & L \\ 0 & 0 & 0 \end{pmatrix}\begin{Bmatrix} J' & L' & \mathscr{J} \\ L & J & l \end{Bmatrix} F^l_{J'\epsilon',J\epsilon} \times [A^l_{J'F_i'\epsilon',JF_i\epsilon}V_{l0}(R)+B^l_{J'F_i'\epsilon',JF_i\epsilon}V_{l2}(R)], \quad \text{(A1)}$$

where l is the index in the expansion of the average and difference of the A' and A'' PESs in Legendre polynomials $P_l^m(\cos\theta)$ with $m=0$ and 2, respectively.[3] In this equation we have defined

$$F^l_{J'\epsilon',J\epsilon} = \tfrac{1}{2}[1-\epsilon\epsilon'(-1)^{J+J'+l}], \quad \text{(A2)}$$

$$A^l_{J'F_i'\epsilon',JF_i\epsilon} = C^{1/2}_{J'F_i'\epsilon'}C^{1/2}_{JF_i\epsilon}\begin{pmatrix} J' & l & J \\ -1/2 & 0 & 1/2 \end{pmatrix} - C^{3/2}_{J'F_i'\epsilon'}C^{3/2}_{JF_i\epsilon}\begin{pmatrix} J' & l & J \\ -3/2 & 0 & 3/2 \end{pmatrix}, \quad \text{(A3)}$$

and

$$B^l_{J'F_i'\epsilon',JF_i\epsilon} = \epsilon\left[C^{1/2}_{J'F_i'\epsilon'}C^{3/2}_{JF_i\epsilon}\begin{pmatrix} J' & l & J \\ -1/2 & 2 & -3/2 \end{pmatrix} - C^{3/2}_{J'F_i'\epsilon'}C^{1/2}_{JF_i\epsilon}\begin{pmatrix} J' & l & J \\ -3/2 & 2 & -1/2 \end{pmatrix}\right]. \quad \text{(A4)}$$

The above equations correct typographical errors in our previous paper[18] on $^2\Pi$ [case (b)] inelastic collisions.[56]

In the centrifugal decoupling (coupled-states) approximation,[37,44] the potential matrix elements are given by[2]

$$\langle J'F_i'\epsilon'P'\mathscr{J}\mathscr{M}|V|JF_i\epsilon P\mathscr{J}\mathscr{M}\rangle = (-1)^{P-1/2}\delta_{P',P}[(2J+1)(2J'+1)]^{1/2} \times \sum_l \begin{pmatrix} J' & l & J \\ -P & 0 & P \end{pmatrix} F^l_{J'\epsilon',J\epsilon}[A^l_{J'F_i'\epsilon',JF_i\epsilon}V_{l0}(R) + B^l_{J'F_i'\epsilon',JF_i\epsilon}V_{l2}(R)]. \quad \text{(A5)}$$

[1] For a review, see P. J. Dagdigian, in *Dynamics and Kinetics of Small Radicals*, edited by K. Liu and A. F. Wagner (to be published).
[2] M. H. Alexander, J. Chem. Phys. **76**, 5974 (1982).
[3] M. H. Alexander, Chem. Phys. **92**, 337 (1985).
[4] R. Schinke and P. Andresen, J. Chem. Phys. **81**, 5644 (1984).
[5] D. P. Dewangan, D. R. Flower, and G. Danby, J. Phys. B **19**, L747 (1986).
[6] D. P. Dewangan, D. R. Flower, and M. H. Alexander, Mon. Not. R. Astron. Soc. **226**, 505 (1987).
[7] G. C. Corey and M. H. Alexander, J. Chem. Phys. **88**, 6931 (1988).
[8] T. Orlikowski and M. H. Alexander, J. Chem. Phys. **79**, 6006 (1983).
[9] H. Joswig, P. Andresen, and R. Schinke, J. Chem. Phys. **85**, 1904 (1986).
[10] G. C. Corey and M. H. Alexander, J. Chem. Phys. **85**, 5652 (1986).
[11] M. H. Alexander, J. Chem. Phys. **99**, 7725 (1993).
[12] M. H. Alexander, W. R. Kearney, and A. F. Wagner, J. Chem. Phys. **100**, 1338 (1994).
[13] B. Pouilly and M. H. Alexander, J. Chem. Phys. **88**, 3581 (1988).
[14] H.-J. Werner, B. Follmeg, M. H. Alexander, and D. Lemoine, J. Chem. Phys. **91**, 5425 (1989).
[15] P. J. Dagdigian, D. Patel-Misra, A. Berning, H.-J. Werner, and M. H. Alexander, J. Chem. Phys. **98**, 8580 (1993).
[16] A. Berning and H.-J. Werner, J. Chem. Phys. **100**, 1953 (1994).
[17] J. M. Brown, J. T. Hougen, K.-P. Huber, J. W. C. Johns, I. Kopp, H. Lefebvre-Brion, A. J. Merer, D. A. Ramsay, J. Rostas, and R. N. Zare, J. Mol. Spectrosc. **55**, 500 (1975).
[18] P. J. Dagdigian, M. H. Alexander, and K. Liu, J. Chem. Phys. **91**, 839 (1989).
[19] A. F. Wagner, T. H. Dunning, Jr., and R. A. Kok, J. Chem. Phys. **100**, 1326 (1994).
[20] R. G. Macdonald and K. Liu, J. Chem. Phys. **91**, 821 (1989).
[21] M. H. Alexander, P. Andresen, R. Bacis, R. Bersohn, F. J. Comes, P. J. Dagdigian, R. N. Dixon, R. W. Field, G. W. Flynn, K.-H. Gericke, B. J.

Howard, J. R. Huber, D. S. King, J. L. Kinsey, K. Kleinermanns, A. C. Luntz, A. J. MacCaffery, B. Pouilly, H. Reisler, S. Rosenwaks, E. Rothe, M. Shapiro, J. P. Simons, R. Vasudev, J. R. Wiesenfeld, C. Wittig, and R. N. Zare, J. Chem. Phys. **89**, 1749 (1988).
[22] D. Secrest, J. Chem. Phys. **62**, 710 (1975).
[23] S. M. Ball, G. Hancock, and M. R. Heal, J. Chem. Soc. Faraday Trans. **90**, 523 (1994).
[24] S. M. Ball, G. Hancock, and M. R. Heal, J. Chem. Phys. Faraday Trans. **90**, 1467 (1994).
[25] P. Heinrich, Ph.D. thesis, Ruhr Universität, Bochum, Germany (1993); P. Heinrich and F. Stuhl, J. Chem. Phys. (submitted).
[26] F. Winterbottom and H. Reisler (unpublished).
[27] M. H. Alexander, S. Gregurick, P. J. Dagdigian, G. W. Lemire, M. J. McQuaid, and R. C. Sausa, J. Chem. Phys. **101**, 4547 (1994).
[28] M. H. Alexander, S. Gregurick, and P. J. Dagdigian, J. Chem. Phys. **101**, 2887 (1994).
[29] I. V. Lebed, E. E. Nikitin, and S. Y. Umanskii, Opt. Spectrosc. (USSR) **43**, 378 (1977).
[30] J. T. Hougen, Natl. Bur. Stand. (U.S.) Monogr. **115** (1970).
[31] R. N. Zare, A. L. Schmeltekopf, W. J. Harrop, and D. L. Albritton, J. Mol. Spectrosc. **46**, 37 (1973).
[32] H. Lefebvre-Brion and R. W. Field, *Perturbations in the Spectra of Diatomic Molecules* (Academic, New York, 1986).
[33] G. Herzberg, *Spectra of Diatomic Molecules*, 2nd ed. (Van Nostrand, Princeton, 1968).
[34] P. F. Bernath, C. R. Brazier, T. Olsen, R. Hailey, W. T. M. L. Fernando, C. Woods, and J. L. Hardwick, J. Mol. Spectrosc. **147**, 16 (1991).
[35] See, for example, D. Secrest, in *Atom–Molecule Collision Theory: A Guide for the Experimentalist*, edited by R. B. Bernstein (Plenum, New York, 1979), p. 265.
[36] C. F. Curtiss and F. T. Adler, J. Chem. Phys. **20**, 249 (1952).
[37] P. McGuire and D. J. Kouri, J. Chem. Phys. **60**, 2488 (1974).
[38] R. T Pack, J. Chem. Phys. **60**, 633 (1974).
[39] J. Tennyson and B. T. Sutcliff, J. Chem. Phys. **77**, 4061 (1982).
[40] J. M. Hutson, in *Advances in Molecular Vibrations and Collision Dynamics*, edited by J. M. Bowman and M. A. Ratner (JAI, Greenwich, CT, 1991), Vol. 1A, p. 1.
[41] M.-L. Dubernet, D. Flower, and J. M. Hutson, J. Chem. Phys. **94**, 7602 (1991).
[42] D. J. Kouri, T. G. Heil, and Y. Shimoni, J. Chem. Phys. **65**, 226 (1976).
[43] D. M. Brink and G. R. Satchler, *Angular Momentum*, 2nd ed. (Clarendon, Oxford, 1968).
[44] D. J. Kouri, in *Atom–Molecule Collision Theory: A Guide for the Experimentalist*, edited by R. B. Bernstein (Plenum, New York, 1979), p. 301.
[45] H. Klar, J. Phys. B **6**, 2139 (1973).
[46] G. W. Lemire, M. J. McQuaid, A. J. Kotlar, and R. C. Sausa, J. Chem. Phys. **99**, 91 (1993).
[47] HIBRIDON is a package of programs for the time-independent quantum treatment of inelastic collisions and photodissociation written by M. H. Alexander, D. E. Manolopoulos, H.-J. Werner, and B. Follmeg, with contributions by P. F. Vohralik, D. Lemoine, G. Corey, B. Johnson, T. Orlikowski, W. Kearney, A. Berning, A. Degli-Esposti, C. Rist, and P. Dagdigian.
[48] E. E. Nikitin and S. Y. Umanskii, *Theory of Slow Atomic Collisions* (Springer, Berlin, 1984).
[49] S. L. Holmgren, M. Waldman, and W. Klemperer, J. Chem. Phys. **67**, 4414 (1977).
[50] C. J. Astbury, G. Hancock, and K. G. McKendrick, J. Chem. Soc. Faraday Trans. **89**, 405 (1993).
[51] M. S. Child, *Molecular Collision Theory*, 2nd ed. (Academic, New York, 1974).
[52] The subroutine ODEINT was employed [W. H. Press, B. P. Flannery, S. A. Teukolsky, and W. T. Vetterling, *Numerical Recipes* (Cambridge University, Cambridge, 1989), Sec. 15.2].
[53] G. Hancock and M. R. Heal, J. Chem. Soc. Faraday Trans. **88**, 2121 (1992).
[54] For a good review, see *Molecular Photodissociation Dynamics*, edited by M. N. R. Ashfold and J. Baggott (Royal Society of Chemistry, London, 1987).
[55] R. Schinke, *Photodissociation Dynamics* (Cambridge University, Cambridge, UK, 1992), see Chap. 11, and references contained therein.
[56] Notwithstanding the errors in the displayed equations, the values of the A and B coefficients reported in Tables I and IV of that paper are correct.